New Coefficient to Characterize Energy Losses in Compressible Flow at T-Junctions

J. Pérez-García, E. Sanmiguel-Rojas* and A. Viedma

Department of Thermal and Fluid Engineering
Universidad Politécnica de Cartagena, E.T.S.I.I. C/ Doctor Fleming, s/n 30202 Cartagena, Spain
* *Departament of Mining and Mechanical Engineering.*
Campus Las Lagunillas 23071, Jaén, Spain.

Abstract

A new coefficient to characterize the global behaviour of adiabatic compressible flow at T-junctions is proposed. The new coefficient is defined according to the conclusions derived from the uncertainty propagation analysis of the total pressure loss coefficient defined by Miller for compressible flow. The numerical results obtained using the new *linking between branches* coefficient definition, $\hat{K}$, show a logarithmic relationship with mass flow rate ratio between branches, q, and the extrapolated Mach number in the common branch, M_3^*, for all flow types studied in a 90 degree T-junction. Reliable and practical two parameters or *global* correlations, $\hat{K} = \hat{K}(M_3^*, q)$, have been obtained. These correlations can be easily implemented as boundary conditions into 1-D global simulation codes.

Keywords: Compressible flow, T-Junctions, Numerical simulation, Loss coefficient definition, Linking coefficient definition, Uncertainty propagation

Notation

a	Non-dimensional parameter $a=(\gamma-1)/2$
b	Non-dimensional parameter $b=\gamma/(\gamma-1)$
c	Non-dimensional parameter $c=(\gamma+1)/2$
D	Internal diameter (m)
f_D	Friction factor (dimensionless) $f_D=4f_{Fanning}$
G	Mass flow rate (kg/s)
h_0	Stagnation enthalpy (J/kg)
h	Static enthalpy (J/kg)
K	Total pressure loss coefficient defined by Miller [31] (dimensionless)
$\hat{K}$	New *linking between branches coefficient* definition (dimensionless)
k_{abs}	Absolute material roughness (m)
L/D	Non-dimensional distance (ratio distance/internal diameter)
L_j	Length of the branch j (m)
ln	Natural logarithm
M	Mach number (dimensionless)
M^*	Extrapolated Mach number up to the junction (dimensionless)
m,n,s	Parameter in the numerical correlations (of the new coefficient definition $\hat{K}$)
p_0	Stagnation pressure (Pa)
p	Static pressure (Pa)
p^*	Extrapolated static pressure up to the junction (after subtracting friction losses) (Pa)
p_0^*	Extrapolated stagnation pressure up to the junction (Pa)
p_t	Total pressure (Pa) $p_t=p+\frac{1}{2}\rho u^2$
q	Mass flow rate ratio between branches (dimensionless) $q=G_2/G_3$

q'	Complementary mass flow rate ratio (dimensionless) $q' = 1 - q = G_1 / G_3$
R^2	Correlation coefficient (dimensionless)
Re	Reynolds number (dimensionless)
R_g	Gas constant (m^2/s^2K)
r_0	Radius of curvature of the internal interface of the branches
S	Cross-sectional area (m^2)
T	Static temperature (K)
T_0	Stagnation temperature (K)
T_0^*	Extrapolated stagnation temperature up to the junction $\left(T_0^* = T_0\right)$ in adiabatic fluid flow condition (K)
U	Expanded uncertainty
u	Standar uncertainty
u_c	Combined standar uncertainty
u_τ	Friction velocity (m/s)
v_j	Velocity in a section of the branch j
x	Distance along each branch (m)
y^+	Sublayer scaled distance (dimensionless) $y^+ = u_\tau y / \nu_w$

Greek symbols

ε	Non-dimensional roughness
ϕ_j	Ratio of extrapolated absolute static pressure (dimensionless) $\phi_j = p_j^* / p_3^*$
ψ	Generic fluid property
γ	Ratio of specific heats (dimensionless) $\gamma = c_p / c_v$
μ	Absolute viscosity (Pa.s)
ρ	Gas density (kg/m^3)
τ_w	Wall shear stress (Pa) $\tau_w = \rho u_\tau^2$
θ	Angle between branches (dimensionless)

Superscripts

*	Extrapolated flow properties to the junction (once friction losses have been subtracted)

Subscripts

1,2	Inlet (combining flows) or outlet (dividing flows) branches
3,c	Common branch
C	Combining flow
D	Dividing flow
d	Downstream
i	Test section in each branch $i = 1, 2, \ldots\ldots N$
j	Branch $j = 1, 2, 3$
J	Junction section
M	Measurement section
u	Upstream
o	Stagnation magnitude
CI	Confidence interval

1. Introduction

T-junctions are present in many fluid piping systems, such as pneumatic fluid power, transport piping, inlet and exhaust in internal combustion engines and compressors, steam and gas turbines, ejectors and mixers in chemical plants and secondary air systems in gas turbines and rocket engines. Steady and transient compressible internal flow simulation models may assist in the analysis and design of these systems. In most global simulation codes, one dimensional flow (1-D) is assumed in straight ducts. However, the flow at junctions and other components is three-dimensional (3-D) and special care is required at such singular elements.

Different modelling techniques of fluid flow in junctions were compared by Basset *et al*. [1] and they concluded that although the multi-dimensional junction model provided better predictions, the pressure loss junction model could predict well if it was used properly. So, a wave action 1-D global simulation model combined with a pressure loss model as boundary condition at the junctions was generally more efficient, since it provides satisfactory results with a lower computational cost. Another alternative is to use a multi-code approach based on the simultaneous use of zero, one- and three-

dimensional models for the different components of the system, Onorati *et al* [2] Chiatti and Chiavola [3] and Kesgin [4], but in this case the computational cost is higher.

In summary, the 1-D models used in the global simulation of steady and transient compressible flow in pipe systems, such as BOOST (AVL) [5], GT-POWER [6], GASDYN [7], ENGINE CARD [8] and others require reliable data of pressure loss coefficients to characterize the overall behaviour of the flow at junctions.

There are numerous experimental data on incompressible flow at junctions. The most reliable and complete reference data are: Miller [9], 73022 and 73023 ESDU items [10][11] and Idelchick [12]. Some recent works, such as Sierra-Espinosa *et al*. [13][14], Adechy and Issa [15], Christian *et al*. [16], Oka and Ito [17] and Costa *et al*. [18] demonstrate the interest of the topic studied. In these works, different aspects of the flow behaviour and methodologies to discount the friction losses, obtain the extrapolated flow properties up to the junction and then calculate the loss coefficient have been established. Also different definitions of the loss coefficient have been proposed and the results have been represented as function of flow rate ratio between branches. Additionally, more complex phenomenon have been studied: de Tilly and Sousa [19] described the unsteady flow behaviour at low mass flow rate ratios in non-isothermal flows, numerical investigations of industrial interest using commercial codes [20] [21], and more recently the combined experimental and numerical study about passive scalar transport in X-junction in incompressible flow was accomplished by Vicente *et al.* [22].

The incompressible flow behaviour at junctions has also been studied through numerical simulation. The most noticeable works using specific codes correspond to Leschziner and Dimitriadis [23] and Zhao and Winterbone [24]. Commercial codes have also been used by different authors: Shaw *et al*. [25] and Gan and Riffat [26]. Finally,

some approximate analytical expressions have been obtained assuming steady, incompressible and uniform flow hypothesis in Navier-Stokes equation system in integral form, Hager [27], Abou-Haidar and Dixon [28], Basset *et al*. [29] and Winterbone and Pearson [30].

In compressible flow the available data are scarce. The only reliable data published in the open literature are the experimental data obtained for commercial T- and Y-junctions by Morimune *et al*. [31] and the experimental investigations on T-and Y-junctions with different angles between branches accomplished by Abou-Haidar and Dixon [32] . In the first work, a *graphical* extrapolation procedure was used to subtract the friction losses and to obtain the extrapolated flow properties up to the junction departing from the measured static pressure at multiple locations in each branch. In the second work, Abou-Haidar and Dixon subtracted the frictional losses in straight duct, between measurement locations and junction, using a procedure only suitable for incompressible flow. In both works, the measurement sections were located close to the junction (between 2D and 30D). In this region the fluid flow is not fully developed and the static pressure gradient used to calculate the non-dimensional friction coefficient is influenced by the junction. Abou-Haidar [33] also studied some combining flow types by numerical simulation using a 2-D specific code. In conclusion, the available data should be contrasted and a more reliable methodology for discounting the frictional losses in compressible flow should be developed.

A new numerical simulation methodology for obtaining the overall loss coefficient at junctions in compressible flow was developed and experimentally validated by Perez-Garcia *et al*. [34]. This methodology consists in carrying out numerical simulations of the 3-D compressible fluid flow at T-junctions using the general purpose commercial code FLUENT^{TM} [35] and processing the obtained numerical results

applying the Fanno fluid flow model to subtract friction losses. The numerical results for different flow types and mass flow rate ratios between branches were compared with our own experimental data and also with the published Abou-Haidar and Dixon data [32]. For this purpose the total pressure loss coefficient defined by Miller [36] was used. In general, a good agreement was achieved. However, the results show a significant dispersion and cannot easily be correlated with the extrapolated Mach number in the common branch [37].

In this work a new *linking between branches coefficient* is proposed to characterize the overall behaviour of compressible flow at junctions. The new coefficient is deducted from the findings obtained in the uncertainty propagation analysis of Miller's coefficient definition. The main advantage of this new proposed coefficient is that the results show a logarithmic relationship with the extrapolated Mach number and, therefore, they can be correlated using simple analytical models. The *global correlations* obtained can easily be implemented as boundary condition in global 1-D simulation codes.

The structure of the paper is the following: In section 2, the results of the uncertainty propagation study of the loss coefficient defined by Miller are summarized and the uncertainty amplification sources are identified. The new loss coefficient definition is introduced in Section 3. Section 4 shows the numerical results and the global correlations obtained, as well as their expanded uncertainties and a summary of the main advantages of the proposed coefficient. In the final section some conclusions are drawn. The results of the dimensional analysis of the problem studied are summarized in appendix A. In appendix B, the numerical implementation of the new global correlations is detailed. Finally, the uncertainty of the numerical results is reported in appendix C.

2. Uncertainty Propagation in the Loss Coefficient Defined by Miller

The total pressure loss coefficient for compressible flow defined by Miller [36], Eq. (1), was derived from the traditionally accepted expression for incompressible flow, also proposed by the same author [9]. For incompressible flow this definition has the physical meaning of quantifying the loss of the stagnation pressure rated with the dynamic pressure at the common branch. For compressible flow analogous definition was proposed by Miller, although the physical interpretation is not so direct. Eq. (1) must be particularized for combining flow types doing $d \equiv c$ and for dividing flow types doing $u \equiv c$, where *u*, *d* and *c* indicate *upstream*, *downstream* and *common*, respectively.

$$K_{ud} = \frac{p_{0u}^{*} - p_{0d}^{*}}{p_{0c}^{*} - p_{c}^{*}}. \tag{1}$$

The loss coefficient from Eq. (1) is expressed as a function of stagnation and static pressure extrapolated up to the junction. These quantities cannot be accurately measured and the flow properties are obtained far away from the junction, where they are not perturbed by the junction effect. Later, subtracting the friction losses, the extrapolated quantities can be calculated. In Fig. 1, actual and extrapolated (subtracting friction losses) stagnation pressure evolution are depicted in a dividing flow type.

Other loss coefficient definitions for compressible flow have also been proposed [4][31]. The most significant non-dimensional parameters that must be considered in this problem can be obtained through dimensional analysis (Appendix A). The loss coefficient must be obtained for different Mach numbers and mass flow rate ratios between branches for each flow configuration at T-junctions. In Fig. 2, the notation of the new *linking coefficient* for the studied flow configurations is shown. The loss coefficient defined by Miller was represented as a function of extrapolated Mach number in common

branch at T-junctions with q = constant and for different angles between branches by Abou-Haidar and Dixon [32] and Abou-Haidar [33].

The uncertainty propagation analysis has been carried out for both combining and dividing flow types. In dividing flow types, for instance, Eq. (1) can be written as a function of the extrapolated Mach numbers according to Eq. (2) and (3)

$$K_{31} = \frac{p_{03}^{*} - p_{01}^{*}}{p_{03}^{*} - p_{3}^{*}}, \tag{2}$$

$$K_{31} = \frac{p_{03}^{*}/p_{3}^{*} - p_{01}^{*}/p_{3}^{*}}{p_{03}^{*}/p_{3}^{*} - 1} = \frac{\left(1 + aM_{3}^{*2}\right)^{b} - \left(p_{1}^{*}/p_{3}^{*}\right)\left(1 + aM_{1}^{*2}\right)^{b}}{\left(1 + aM_{3}^{*2}\right)^{b} - 1}, \tag{3}$$

where, *3* is the inlet and common branch, $c \equiv u = 3$, and *1* is the outlet branch, $d = 1$. To calculate the extrapolated quantities it is necessary to obtain, numerically or experimentally, mass flow rate, static temperature and absolute static pressure in both branches involved. So, the loss coefficient K_{31} and its expanded uncertainty can be expressed according to Eq. (4) and (5) respectively,

$$K_{31} = K_{31}(G_3, T_3, p_3, G_1, T_1, p_1), \tag{4}$$

$$U(K_{31}) = U\left(u(G_3), u(T_3), u(p_3), u(G_1), u(T_1), u(p_1)\right), \tag{5}$$

where $u(\psi)$ is the standard uncertainty associated with the uncorrelated input estimate ψ. Previous to determine the combined standard uncertainty of the Miller loss coefficient, it is necessary to obtain the absolute sensitivity coefficients associated to each variable. Using differential calculus and considering that the standard uncertainties of the input magnitudes are uncorrelated, we can derive each branch "1" and "3" separately and then combine according to Eq. (6),

$$\frac{dK_{31}}{K_{31}} = \frac{dK_{31}}{K_{31}}\bigg|_1 + \frac{dK_{31}}{K_{31}}\bigg|_3 . \tag{6}$$

where, differentiating Eq. (3),

$$dK_{31}\big|_1 = \frac{\partial K_{31}}{\partial M_1^*} dM_1^* + \frac{\partial K_{31}}{\partial p_1^*} dp_1^*, \tag{7}$$

$$dK_{31}\big|_3 = \frac{\partial K_{31}}{\partial M_3^*} dM_3^* + \frac{\partial K_{31}}{\partial p_3^*} dp_3^*, \tag{8}$$

organizing terms, Eq. (6) can be written as Eq.(9),

$$\frac{dK_{31}}{K_{31}} = \Lambda_{1D} \frac{dM_1^*}{M_1^*} + \Gamma_{1D} \frac{dp_1^*}{p_1^*} + \Lambda_{3D} \frac{dM_3^*}{M_3^*} + \Gamma_{3D} \frac{dp_3^*}{p_3^*} , \tag{9}$$

where parameters Λ and Γ for each branch, assuming adiabatic flow condition $T_{01}^* = T_{03}^* = T_0 = constant$, are given by:

$$\Lambda_{1D} = -\gamma M_1^{*2} \left(\frac{T_0^*}{T_1^*}\right)^{b-1} \frac{p_1^*}{p_{03}^*} \left[1 + \left(\frac{1}{K_{31}} \frac{p_{01}^*}{p_{03}^* - p_3^*}\right)\right], \tag{10}$$

$$\Lambda_{3D} = \gamma M_3^{*2} \left(\frac{T_0^*}{T_3^*}\right)^{b-1} \frac{p_3^*}{p_{03}^* - p_3^*} \left[\frac{1 - K_{31}}{K_{31}}\right], \tag{11}$$

$$\Gamma_{1D} = 1 - \left(\frac{1}{K_{31}} \frac{p_{01}^*}{p_{03}^* - p_3^*}\right), \tag{12}$$

$$\Gamma_{3D} = \frac{p_3^*}{p_{03}^* - p_3^*} \left[\frac{\left(p_{03}^*/p_3^*\right)(1 - K_{31}) + K_{31}}{K_{31}}\right], \tag{13}$$

Now we must take into account the procedure of extrapolation detailed in [34] to relate the extrapolated and measured quantities Eq. (16). In this procedure the friction coefficient for fully-developed fluid flow region is previously obtained using the Fanno model momentum equation in differential form, Eq. (14)

$$f_{Di} = \frac{2D}{\gamma M_i^3} \frac{1 - M_i^2}{1 + \frac{1}{2}(\gamma - 1) M_i^2} \left. \frac{dM}{dx} \right|_i . \tag{14}$$

To discretize $dM/dx|_i$, by means of finite differences in a non-uniform mesh, the expressions from [38] have been used. Doing $f_{Di} = f_{Di}|_{fully-developed} \cong constant = \bar{f}_D$, the Eq. (14) can be analytically integrated to obtain Eq. (15)

$$\bar{f}_D \frac{(x_i - x_{i-1})}{D} = \frac{1}{\gamma M_i^2} \left(\frac{M_i^2 - M_{i-1}^2}{M_{i-1}^2} \right) + \frac{\gamma + 1}{2\gamma} ln \left[\frac{M_{i-1}^2 \left(2 + (\gamma - 1) M_i^2\right)}{M_i^2 \left(2 + (\gamma - 1) M_{i-1}^2\right)} \right]. \tag{15}$$

This equation links the Mach number with the distance x along the duct, where M_i and M_{i-1} are the averaged Mach numbers in two locations with $x_{i-1} < x_i$, for any branch and where $x = 0$ is the junction. Eq. (15) is used to obtain the extrapolated Mach number in each branch, $j = 1, 2, 3$. Differentiating Eq. (15) at any branch "j", we can obtain a relationship between Mach number in the measurement section M_j, and the extrapolated Mach number M_j^* at the junction,

$$\frac{dM_j^*}{M_j^*} = F_{jD} \frac{dM_j}{M_j}, \tag{16}$$

where F_{jD} (dividing flow types) is given by:

$$F_{jD} = \frac{\frac{1}{M_j^2} - c + \frac{acM_j^2}{\left(1 + aM_j^2\right)}}{\frac{1}{M_j^{*2}} - c + \frac{acM_j^{*2}}{\left(1 + aM_j^{*2}\right)}} . \tag{17}$$

Taking into account now Eq. (18) and (19) we can relate Mach number and stagnation temperature with the fluid properties evaluated in each branch. These equations can be applied to the flow properties, in the initial section and to the extrapolated quantities up to the junction,

$$\frac{dM_j}{M_j} = \frac{1}{2}\frac{dT_j}{T_j} + \frac{dG_j}{G_j} - \frac{dp_j}{p_j} \quad , \tag{18}$$

$$\frac{dT_{0j}}{T_{0j}} = \frac{dT_j}{T_j} + 2\left(1 - \frac{T_j}{T_{0j}}\right)\frac{dM_j}{M_j} \quad . \tag{19}$$

Substituting now Eq. (16), (18) and (19) for $j = 1,3$ in (9), we obtain:

$$\frac{dK_{31}}{K_{31}} = \frac{1}{2}\Delta_{T1D}\frac{dT_1}{T_1} + \Delta_{G1D}\frac{dG_1}{G_1} - \Delta_{p1D}\frac{dp_1}{p_1} + \frac{1}{2}\Delta_{T3D}\frac{dT_3}{T_3} + \Delta_{G3D}\frac{dG_3}{G_3} - \Delta_{p3D}\frac{dp_3}{p_3} \tag{20}$$

where the sensitivity coefficients are,

$$\alpha_{1D} = \left(1 - \frac{T_1}{T_0}\right) - \left(2 - \frac{T_1^*}{T_0}\right)F_{1D} \quad , \tag{21}$$

$$\Delta_{T1D} = \Lambda_{1D}F_{1D} + \Gamma_{1D}(1 + \alpha_{1D}) \quad , \tag{22}$$

$$\Delta_{G1D} = \Lambda_{1D}F_{1D} + \Gamma_{1D}(1 + \alpha_{1D}) \quad , \tag{23}$$

$$\Delta_{p1D} = \Lambda_{1D}F_{1D} + \Gamma_{1D}\alpha_{1D} \quad , \tag{24}$$

$$\alpha_{3D} = \left(1 - \frac{T_3}{T_0}\right) - \left(2 - \frac{T_3^*}{T_0}\right)F_{3D} \quad , \tag{25}$$

$$\Delta_{T3D} = \Lambda_{3D}F_{3D} + \Gamma_{3D}(1 + \alpha_{3D}) \quad , \tag{26}$$

$$\Delta_{G3D} = \Lambda_{3D}F_{3D} + \Gamma_{3D}(1 + \alpha_{3D}) \quad , \tag{27}$$

$$\Delta_{p3D} = \Lambda_{3D}F_{3D} + \Gamma_{3D}\alpha_{3D} \quad . \tag{28}$$

Finally, the combined standard uncertainty $u_c(K_{31})$ is defined as,

$u_c^2(K_{31}) = u_{T1}^2(K_{31}) + u_{G1}^2(K_{31}) + u_{p1}^2(K_{31}) + u_{T3}^2(K_{31}) + u_{G3}^2(K_{31}) + u_{p3}^2(K_{31})$, where, for example, for the magnitude T_1, $u_{T1}(K_{31}) = \frac{\partial K_{31}}{\partial T_1}u(T_1) = \frac{\partial K_{31}}{\partial T_1}dT_1$. We have used in this step the equivalence in notation between standard uncertainty $u(\psi)$ and the differential $d\psi$ of a generic input magnitude ψ. In consequence, the contribution of the T_1 uncertainty on the uncertainty of the result, (K_{31}) can be easily obtained from Eq. (20) considering separately the standard uncertainty $u(\psi)$ of the rest of input magnitudes ψ,

$$u_{T1}(K_{31}) = dK_{31}(dG_1 = dp_1 = dT_3 = dG_3 = dp_3 = 0) = \frac{1}{2}\frac{K_{31}}{T_1}\Delta_{T1D}dT_1$$

Similarly, all the components of the uncertainty of the result $u_{\psi}(K_{31})$ can be obtained from Eq. (20).

Finally, the expanded uncertainty $U(K_{31}) = ku_c(K_{31})$ referred to the 95% confidence interval, in which the coverage factor is $k = 2$, can be obtained from Eq. (29), according to the ISO standard "Guide to the Expression of Uncertainty in Measurement" [39],

$$U(K_{31}) = k\left(u_{T1}^2(K_{31}) + u_{G1}^2(K_{31}) + u_{p1}^2(K_{31}) + u_{T3}^2(K_{31}) + u_{G3}^2(K_{31}) + u_{p3}^2(K_{31})\right)^{1/2} \quad (29)$$

This expression allows us to establish that static pressure uncertainty is amplified in the calculation of the Miller loss coefficient, being its contribution to the expanded uncertainty one order of magnitude higher than the contribution of the static temperature or mass flow rate measurement uncertainties.

The explanation is that this is because Γ and α parameters in the sensitivity coefficients are $\Gamma = O(10)$ and $\alpha = O(-1)$ respectively, in consequence, the uncertainty of the static pressure is amplified, Eq. (24) and (28). On the other hand, the influence of the Γ parameters is counterbalanced in the static temperature, Eq. (22) and (26), and mass flow rate, Eq. (23) and (27), so, these uncertainties are maintained in the same order of magnitude as their initial uncertainties. Finally, in all cases studied the parameters Λ and F are $\Lambda = O(1)$ and $F = O(1)$ which demonstrate that extrapolation procedure do not introduce additional uncertainty, Eq. (16).

Similarly the total uncertainty of loss coefficient K_{32}, and the coefficients K_{13} and K_{23}, for the combining flow types, can be calculated.

3. Proposed New Coefficient

According to the uncertainty propagation study previously accomplished, it can be concluded that the initial uncertainties are not amplified by the extrapolation procedure used to subtract the friction losses. In consequence, the static pressure measurement uncertainty is amplified only due to the coefficient definition itself. Therefore, it would be interesting to define a new coefficient to characterize the flow behaviour at T-junctions avoiding this uncertainty amplification and the subsequent dispersion and irregularity of the results.

In this section a new definition to the loss coefficient is proposed departing from the total pressure loss coefficient defined by Miller. Miller's coefficient can be expressed according to Eq. (30) (in dividing flow types, for instance):

$$K_{3j} = \frac{P_{03}^* - P_{0j}^*}{P_{03}^* - P_3^*} = \frac{f(M_3^*) - \phi \cdot f(M_j^*)}{f(M_3^*) - 1}, \quad j = 1,2 \ , \tag{30}$$

where, $\phi = \frac{P_j^*}{P_3^*} \sim 1$, $f(M_j^*) = (1 + aM_j^{*2})^b$ and $f(M_3^*) = (1 + aM_3^{*2})^b$.

Eq. (30) can be rewritten doing, $x = M_3^*$, $y = M_j^*$, according to Eq. (31):

$$K_{3j} = \frac{1}{g(x)} - \frac{\phi}{h(x,y)}, \tag{31}$$

where, $g(x)$ and $h(x, y)$ are defined from Eq. (32) and (33) respectively:

$$g(x) = \frac{f(x) - 1}{f(x)}, \tag{32}$$

$$h(x, y) = \frac{f(x) - 1}{f(y)}. \tag{33}$$

In Eq. (31) the influence of the Γ and Λ parameters is uncoupled. To avoid the uncertainty amplification, only type Λ parameters will be retained. So, doing partial

derivatives in (31) considering ϕ constant, the uncertainty of Miller's coefficient definition can be related to the uncertainty of $g(x)$ and $h(x, y)$, according to Eq. (34),

$$\left.\frac{dK_{3j}}{K_{3j}}\right|_{\phi=Cte} = -\frac{1}{gK_{3j}}\frac{dg}{g} + \frac{\phi}{hK_{3j}}\frac{dh}{h}, \tag{34}$$

where,

$$\frac{dg}{g} = \frac{2abx^2\left(1+ax^2\right)^{b-1}}{\left(1+ax^2\right)^b - 1}\frac{dx}{x} - \frac{2abx^2\left(1+ax^2\right)^{b-1}}{\left(1+ax^2\right)^b}\frac{dx}{x}, \tag{35}$$

$$\frac{dh}{h} = \frac{2abx^2\left(1+ax^2\right)^{b-1}}{\left(1+ax^2\right)^b - 1}\frac{dx}{x} - \frac{2aby^2\left(1+ay^2\right)^{b-1}}{\left(1+ay^2\right)^b}\frac{dy}{y}. \tag{36}$$

Considering that the uncertainty of the flow properties in each branch is similar, $dx/x \approx dy/y$, and the extrapolated Mach number is of equal order of magnitude and also varies in the same way, $x \approx y$, it can be concluded according to (35) and (36) that the uncertainties of $g(x)$ and $h(x, y)$ are of the same order of magnitude in all studied cases.

$$\frac{dg}{g} \approx \frac{dh}{h}. \tag{37}$$

Substituting (37) in (34), we obtain

$$\left.\frac{dK_{3j}}{K_{3j}}\right|_{\phi=Cte} = -\frac{1}{gK_{3j}}\frac{dg}{g} + \frac{\phi}{hK_{3j}}\frac{dh}{h} \approx -\frac{1}{K_{3j}}\left(\frac{1}{g} - \frac{\phi}{h}\right)\frac{dh}{h} \approx -\frac{dh}{h}. \tag{38}$$

In short, it is important to pointed out that when in Miller's definition we assume ϕ = *constant* the uncertainty is not amplified, and that this hypothesis is only a way of deducing a more suitable loss coefficient definition, but it is not a realistic assumed hypothesis. From Eq. (38) we can conclude that a type function $h(x, y)$ has a similar uncertainty than Miller's loss coefficient definition when ϕ = constant is considered. Then, if a $h(x, y)$ type function is formulated as new coefficient definition, the

uncertainty will not be amplified. So a new improved coefficient to characterize the compressible flow behaviour at T-junctions can be formulated from Eq. (39),

$$\hat{K}_{3j} = \frac{f(M_3^*) - 1}{f(M_j^*)}. \tag{39}$$

In combining flow types the loss coefficient defined by Miller can be related to the new coefficient according to,

$$K_{j3} = \frac{p_{0j}^* - p_{03}^*}{p_{03}^* - p_3^*} = \frac{\phi}{\hat{K}_{j3}} - \frac{f(M_3^*)}{f(M_3^*) - 1}, \qquad j = 1, 2. \tag{40}$$

Both particularized coefficients can be related and defined by a single expression for combining and dividing flow types from Eq. (41), which supposes an important simplification,

$$\hat{K}_{j3} = \frac{f(M_3^*) - 1}{f(M_j^*)} = \hat{K}_{3j} = \hat{K}_j, \tag{41}$$

Since the new coefficient has been deduced using a purely mathematical procedure, it lacks physical significance although this fact is not a problem when it is used to obtain practical correlations implemented later as boundary conditions in 1D global simulation codes. The new coefficient must be interpreted as a *linking between branches* coefficient, since it links the extrapolated flow properties of the involved branches. In following sections, some additional advantages of the new coefficient will be commented on.

4. Results

In previous works [34] [37], it has been observed that the results obtained using the Miller's loss coefficient for compressible flow do not show a clear trend in most flow

types studied. This fact can be observed in both, published data from Abou-Haidar and Dixon and numerical and experimental results obtained by the authors.

4.1 New Coefficient Global Correlations

In [34] the authors provided experimental *partial* correlations for Eq. (1), to fixed mass flow rate ratios of $q = 0, 0.25, 0.5, 0.75 \text{ and } 1$ in both, combining (*C2*) and dividing (*D2*) flow types. These correlations can not be adjusted to any simple mathematical expression and, therefore, it will be difficult to implement as boundary condition in global 1-D simulation codes. To solve this difficulty, we provide in this paper new numerical *global* correlations. The numerical results were obtained using the numerical procedure developed and validated in [34] and the new definition of *linking between branches* coefficient, Eq.(42)

$$\hat{K}_j = \frac{\dfrac{P_{03}^*}{P_3^*} - 1}{\dfrac{P_{0j}^*}{P_j^*}} = \frac{\left(1 + aM_3^{*2}\right)^b - 1}{\left(1 + aM_j^{*2}\right)^b}, \quad j = 1,2, \tag{42}$$

where 3 is the common branch and 1 and 2 are the inlet or outlet branches . The term *linking* coefficient is used to point out that it does not express directly a loss pressure concept, but a relationship between upstream and downstream flow variables.

Numerical results have shown that $\hat{K}_j$ can be globally correlated with $(1+q)$ and M_3^* , according to,

$$ln\left[(1+q)\hat{K}_j\right] = m\,ln\,M_3^* + n\,ln(1+q) + ln(s), \tag{43}$$

where ln is the natural logarithm and m, n and s are parameters obtained by a least minimum square fit procedure , that can be written in the equivalent form,

$$\hat{K}_j = \hat{K}_j\left(M_3^*, q\right) = s\left(M_3^*\right)^m (1+q)^{n-1}. \tag{44}$$

With *global* we mean that only one expression, Eq. (44), is enough to summarize and characterize all the local energy losses at the junction as a function of the two parameters: q and M_3^*. *Partial* correlations for q constant are not necessary. It is also important to mention that only one expression is required for both flow types combining and dividing. This implies an important simplification in reference to others definitions.

4.2 Combining and Dividing Flow Types

In the reference [34] experimental and numerical data were presented for $C2$ and $D2$ flow types using the Miller´s coefficient definition, with the aim to validate both experimental and numerical developed methodologies. Now numerical and experimental results have been compared using the new *linking between branches* coefficient definition. In Figure 3 the experimental results, regression plane and numerical results are represented in linear scale. In Figure 3 a) the results for combining flow type C2 are compared. Numerical results were obtained for extrapolated Mach number $M_3^* > 0.2$ while experimental test were accomplished also in incompressible flow. It can be observed a good agreement between experimental data and numerical results for all mass flow rate ratios between branches. The results for dividing flow type D2 are compared in Figure 3 b). In this flow configuration the interval of extrapolated Mach number experimentally tested is lower than numerically, due to limitations in the flow bench facility, and the agreement between experimental and numerical results is also excellent in all mass flow rate ratios studied.

These numerical simulations have been completed and now original numerical results for combining flow $C1$ and dividing flow $D1$ are included. In Fig. 4a) and 4c) the regression planes given by Eq. (44) and the values obtained for the new linking coefficient $\hat{K}_2$ at the combining $C2$ and dividing $D2$ flow types have been represented.

The numerical results show a very good linear adjustment when logarithmic axes are used, as can be observed in the projected view in the Fig. 4 b) and d). In Fig. 5 the regression planes for the coefficients $\hat{K}_1$ and $\hat{K}_2$ and the experimental values for combining flow type $C1$ and dividing flow type $D1$ are represented.

Global correlations for both coefficients $\hat{K}_1$ and $\hat{K}_2$, and their expanded uncertainties (95% confidence interval) obtained according to Coleman and Steele procedure detailed in [40], are summarized in Table 1.

The range of applicability of the proposed correlations must be expressed in terms of extrapolated Mach number in the common branch and mass flow rate ratio. The numerical simulations test have been accomplished in the interval $0.15 \le M^*_3 \le 0.7$ and for mass flow rate ratios of $q = 0,0.25,0.5,0.75$ and 1 (observe that M^*_3 is the extrapolated Mach number at the junction after subtracting the frictional losses, and this interval can correspond to a different physical Mach number interval depending on the length of each branch, surface roughness, etc). In consequence, the proposed correlations can be accurately applied in this interval. However, taking into account the excellent linearity of the regression planes, this interval could be reliability extended.

It is worth to mention that in $C2$ and $D2$ flow types, only one global correlation is required, respectively. In Table 1 the correlations for the coefficient $\hat{K}_2$ are proposed. These correlations can be used for the coefficients $\hat{K}_1$ substituting q by $q' = (1 - q)$.

The regression coefficient R-square denominated coefficient of multiple determinations [41] is also reported.

The obtained global correlations constitute a very useful numerical tool, since they can be easily implemented as boundary condition in 1D global simulations codes. This type of boundary condition provides continuous information calculating the linking coefficient between extrapolated flow properties at the junction. Global correlations are adequate for each flow configuration and they can also be applied in unsteady compressible flows in which the mass flow rate ratio is changing continuously.

The numerical implementation of the numerical correlations is detailed in Appendix B, and finally the uncertainty of the numerical results has been assessed in Appendix C, according to the procedure propose in [42].

4.3 Advantages of the New Coefficient Definition

The proposed new coefficient has important advantages compared to the loss coefficient defined by Miller:

- The new coefficient shows a linear relationship with the extrapolated Mach number in the common branch for $q = cte$ when represented in a double logarithmic scale. This fact allows us to obtain reliable and accurate correlations with lower computational or experimental effort, since the numerical simulations or experimental tests required are greatly reduced.
- The proposed coefficient is more sensitive in reference to the Mach number.
- The expanded uncertainty of the *linking between branches* coefficient is similar to the uncertainty of the initial numerical results or experimental measurements, since the new definition does not amplify these uncertainties.
- The new definition is the same for both combining and dividing flow types.

- Finally, simple and compact expressions can be obtained to correlate the $\hat{K}$ with the mass flow rate ratio and extrapolated Mach number. These correlations can be easily implemented as boundary conditions in global 1D simulation codes, avoiding complex interpolation routines. So, the problem of the database discretization can be reduced to the flow configuration level.

The new coefficient has the disadvantage of its low sensitivity to the mass flow rate ratio between branches, although this inconvenience was also observed in the loss coefficient defined by Miller, therefore it could be intrinsic to the fluid flow behaviour at junctions. Besides, the *linking coefficient* does not have a clear physical significance as energy loss coefficient of the flow, although in terms of its practical utilization as boundary condition this inconvenience is not relevant.

Conclusions

A detailed analysis of the uncertainty propagation in the calculation of the loss coefficient in compressible flow at T-junctions has been accomplished. It has been detected that when Miller's definition is used, the static pressure measurement uncertainty is amplified. The influence of the uncertainties of the rest of the flow properties, such as, mass flow rate or static temperature, is less important because their uncertainties are not amplified.

Uncertainty propagation due to the data processing methodology for obtaining the extrapolated flow properties up to the junction, according to the Fanno fluid flow model, has also been analyzed and it is concluded that no meaningful uncertainties are introduced. In consequence, the origin of this uncertainty amplification is the loss coefficient definition itself.

In order to minimize the uncertainty propagation in the calculation of loss coefficient and to reduce the observed data dispersion when Miller's loss coefficient is used a new coefficient definition is proposed. This new *linking between branches* coefficient links the extrapolated Mach number in both involved branches, and provides some interesting advantages, such as, a logarithmic relationship with the extrapolated Mach number in common branch. So, the number of required experimental tests or numerical simulations to characterize its dependence is greatly reduced. In addition, the loss coefficient can be obtained accurately inside a wider Mach number interval by extrapolation. The proposed new coefficient is also more sensitive to the Mach number variations providing consistent results for different flow configurations and different mass flow rate ratios. Finally, it is interesting to emphasize that the same definition is valid for combining and dividing flows.

Finally, the proposed new coefficient allows us to obtain two parameter or global correlations, which constitute a powerful tool to characterize the global flow behaviour at T-junctions. The regression global uncertainty for each proposed correlation has also been estimated and the higher uncertainty is about $6.25\,\%$.

Acknowledgements

This research has been supported by Seneca project PB/19/FS/97 of Comunidad Autónoma de la Región de Murcia (experimental facilities), and by Ministerio de

Educación y Ciencia of Spain (grants DPI2003-02719, DPI2005-08654-C04-01 and TRA2006-15015). The numerical simulations have been made in the computer facilities at the SAIT (Universidad Politécnica de Cartagena).

Appendix A. Dimensional Analysis

The most significant non-dimensional parameters to be considered in this study can be obtained through dimensional analysis. The "jump" of extrapolated stagnation pressures depends on the indicated flow properties in Eq. (A.1), when the hypothesis of steady, compressible and adiabatic internal flow in a constant circular cross-sectional can be assumed. In combining flow types with, $d \equiv c$,

$$p_{0u}^{*} - p_{0c}^{*} = f\left(G_u, G_c, \mu, \gamma, R_g, T_0, \rho_c^{*}, r_0, D_u, D_c, \theta, k_{abs}\right). \tag{A.1}$$

It can be expressed in non-dimensional form according to Eq. (A.2),

$$\frac{p_{0u}^{*} - p_{0c}^{*}}{\gamma M_c^{*2} p_c^{*}} = \varphi_1\left(q, Re_c^{*}, \gamma, M_c^{*}, \frac{r_0}{D_c}, \frac{D_u}{D_c}, \theta, \frac{k_{abs}}{D_c}\right). \tag{A.2}$$

On the other hand, the denominator in Eq. (1) can also be expressed as Eq. (A.3),

$$p_{0c}^{*} - p_c^{*} = p_c^{*}\left[\left(1 + \tfrac{\gamma-1}{2} M_c^{*2}\right)^{\frac{\gamma}{\gamma-1}} - 1\right] = p_c^{*}\varphi_2\left(M_c^{*}\right). \tag{A.3}$$

Taking into account Eq. (A.2) and (A.3) and simplifying, we obtain:

$$\frac{p_{0u}^{*} - p_{0c}^{*}}{p_{0c}^{*} - p_c^{*}} = \frac{\gamma M_c^{*2} p_c^{*}}{p_c^{*}} \frac{\varphi_1}{\varphi_2} = \varphi\left(M_c^{*}, q, Re_c, \gamma, \frac{r_0}{D_c}, \frac{D_u}{D_c}, \theta, \frac{k_{abs}}{D_c}\right). \tag{A.4}$$

Equation A.4 can be simplified according to Eq. (A.5) when: geometrical similitude between T-junctions is achieved, the effect of the relative roughness is negligible, the specific heat is constant in the studied range and the test fluid is air in all cases.

$$\frac{p_{0u}^{*} - p_{0c}^{*}}{p_{0c}^{*} - p_c^{*}} = \varphi\left(M_c^{*}, q, Re_c^{*}\right). \tag{A.5}$$

The extrapolated Reynolds number in common Branch Re_c^* is about 10^5 in all experimental tests and numerical simulations. In this range its influence in the loss coefficient is negligible, see for instance [9][10][11][17][28][31].

Appendix B. Implementation of the new experimental correlations

In this section, we summarize the algorithm used in the most of 1-D models and the introduction of the new correlations as boundary conditions at the junction. For instance, we apply the algorithm to dividing flow type *D2* (see Fig. 1) governed by the following equation system:

$$G_1 - \rho_1 v_1 \frac{\pi D^2}{4} = 0, \tag{B.1}$$

$$M_1 - \frac{v_1}{\sqrt{\gamma R_g T_1}} = 0, \tag{B.2}$$

$$\rho_1 - \frac{P_1}{R_g T_1} = 0, \tag{B.3}$$

$$T_0 - T_1\left(1 + aM_1^2\right) = 0, \tag{B.4}$$

$$\gamma \frac{f_D L_j}{D} - \frac{1}{M_j^2}\left(\frac{M_j^2 - M_j^{*2}}{M_j^{*2}}\right) - c\,ln\left[\frac{M_j^{*2}\left(1 + aM_j^2\right)}{M_j^2\left(1 + aM_j^{*2}\right)}\right] = 0, \quad \text{j=1,2,3} \tag{B.5}$$

$$q + q' - 1 = 0, \tag{B.6}$$

$$q' - \frac{G_1}{G_3} = 0, \tag{B.7}$$

$$\frac{\left(1 + aM_3^{*2}\right)^b - 1}{\left(1 + aM_1^{*2}\right)^b} - sM_3^{*m}\left(1 + q'\right)^{n-1} = 0, \tag{B.8}$$

$$\frac{\left(1 + aM_3^{*2}\right)^b - 1}{\left(1 + aM_2^{*2}\right)^b} - sM_3^{*m}\left(1 + q\right)^{n-1} = 0, \tag{B.9}$$

where (B.5) is the momentum equation in each branch, see [34], (B.6) is the continuity equation at the junction, (B.8) and (B.9) are $\hat{K}_1$ and $\hat{K}_2$ correlations, respectively, that in the case of *D2* configuration (symmetrical flow type), *s*, *m* and *n* are the same for both, see Table 1. In other non-symmetrical flow types such as *C1* and *D1* the correlations for both coefficients are different.

The equation system (B.1)-(B.9) has *11* equations and *15* unknowns, therefore, is necessary to impose *4* unknowns that, in the most of the commercial numerical codes, are T_0, G_3, P_1 and q. After imposing these *4* values, the equation system can be formally written as:

$$F(\vec{x}) = 0, \tag{B.10}$$

where, $\vec{x} = \left[G_1 \ \rho_1 \ v_1 \ T_1 \ M_1 \ M_1^* \ M_2 \ M_2^* \ M_3 \ M_3^* \ q'\right]^T$, is the unknown vector.

This equation system is non-linear, therefore, is necessary to use iterative techniques. One of the most popular techniques to solve non-linear equation systems is the Newton-Raphson method that, basically, can be summarized at each *k*-iteration as:

$$\delta\vec{x}^k = -\left[J(\vec{x}^{k-1})\right]^{-1} F(\vec{x}^{k-1}), \tag{B.11}$$

$$x^k = x^{k-1} + \delta\vec{x}^k, \tag{B.12}$$

with, $J(\vec{x}^k)$, the Jacobian matrix at the *k*-iteration, and $\delta\vec{x}^k$ the correction in each *k*-iteration, see [43] for more details about the Newton-Raphson method. Once $\vec{x}$ is obtained, all the remains fluid magnitudes can be calculated at the branches 2 and 3. A similar methodology can be applied in configurations with multiple junctions.

Appendix C. Uncertainty of Numerical Results

Systematic grid refinement studies are the most common approach used in assessing the numerical accuracy of a numerical simulation. In this work, the proposed approach by Freitas *et al*. [42] to estimate the numerical results uncertainty has been applied.

If the formal order of accuracy is not known, then three different grids and their results are required to determine the order of the method and the error. The ratio of grid spacing or proportionality ratio between cells may be any real number when the Grid Convergence Index (GCI) is calculated to estimate the uncertainty due to discretization errors.

To accomplish the grid dependence study, the Mach number in a fixed location of the computational domain has been calculated using three different refined meshes. The ratio of grid spacing in the cells adjacent to the wall of the three grids is $r = 2$. The simulations were accomplished for different mass flow ratios at flow type *C2* and mass flow rate ratio $q = 0.5$ was maintained constant. In table C.1, the geometrical characteristics of the three meshes studied are summarized. In table C.2, the results obtained in estimating the numerical uncertainty are shown. The evaluated case is a combining flow type *C2*, $q = 0.5$ and mass flow rate 0.064 kg/s in each inlet branch. The

numerical simulations were carried out for the three grids and different mass flow rates: 0.016, 0.024, 0.04, 0.056, 0.064, 0.088 and 0.1 kg/s.

The numerical uncertainty decreases significantly when the numerical results obtained with the *normal* and *fine* meshes are compared. The calculated values for different mass flow rates are similar in both actual p and $p = 1$. This parameter p is defined in [42] as the apparent order of the method. It can be concluded that the obtained results with *normal* mesh are reliable and the computational cost is lower than when the *fine* mesh is used, in consequence the *normal* mesh will be used systematically in all numerical simulations.

Finally, in table C.3 the obtained values of GCI (%) for Mach number in common branch at the distance $L/D = 40.25$ from the junction and different mass flow rates studied are summarized. It can be observed that numerical uncertainty increases when the mass flow rate increases, although the GCI_{fine} values are maintained, in all cases, inside $1.2\,\%$ accuracy interval.

References

[1] M.D. Basset, D.E. Winterbone, R.J. Pearson, Modelling engines with pulse converted exhaust manifolds using one-dimensional techniques, SAE Technical paper series 2000-01-0290 (2000).

[2] A. Onorati, G. Ferrari, G. D'Errico, The Coupling of 1D and 2D Fluid Dynamic Models fro the Prediction of Unsteady Flows in I.C Engine Duct-Systems, IMechE Int. Conf. "Computational and Experimental Methods in Reciprocating Engines" (2000)

[3] G. Chiatti, O. Chiavola, Multi-code prediction of the influence of the exhaust system on the performance of a turbocharged engine, Journal of Engineering for Gas Turbines and Power 124 3 (2002) 695-701.

[4] U. Kesgin, Study on the design of inlet and exhaust system of a stationary internal combustion engine, Energy Conversion and management 46 (2005) 2258-2287.

[5] BOOST, User Manual for AVL BOOST, AVL List GmbH, Department for Applied Thermodynamics, 1996 (http://www.avl.com)

[6] GT Power. Gamma Technologies (http://www.gtisoft.com)

[7] GASDYN. Department of Energetics. Politecnico di Milano (Italy). (http://engines.polimi.it/GASDYN.html)

[8] ENGINE CARD. Thermal Systems Research and Modelling Group. Technical University of Valencia (Spain). (http://www.imst.upv.es/software-propio.php)

[9] D.S. Miller, Internal Flow – A guide to losses in pipe and duct systems, 2nd Ed., BHRA (1971).

[10] ESDU 73022, Pressure losses coefficients in three-leg pipe junctions: dividing flows, ESDU International plc., London (1973).

[11] ESDU 73023, Pressure losses coefficients in three-leg pipe junctions: combining flows, ESDU International plc., London (1973).

[12] I.E. Idelchik, Handbook of hydraulic resistance. 3rd Ed., New York, Begell House, Inc. (1996).

[13] F.Z. Sierra-Espinosa, C.J. Bates, T. O'Doherty, Turbulent flow in a 90º pipe junction. Part 1. Decay of fluctuations upstream the flow bifurcation, Computer & Fluids 29 (2000) 197-213.

[14] F.Z. Sierra-Espinosa, C.J. Bates, T. O'Doherty, Turbulent flow in a 90º pipe junction. Part 2. Reverse flow at the branch exit, Computer & Fluids 29 (2000) 215-233.

[15] D. Adechy, R.I Issa, Modelling of annular flow through pipes and T-junctions, Computer & Fluids 33 (2004) 289-313.

[16] A. Christian, A. Selamet, K.D. Miazgowicz, K.V. Tallio, Flow losses at circular T-junctions representative of intake plenum and primary runner interface, SAE Technical paper series 2004-01-1414 (2004).

[17] K. Oka, H. Ito, Energy losses at tees with large area ratios. Trans. ASME, J. of Fluid Engineering, 127 (2005) 110-116.

[18] N.P. Costa, R. Maia, P.T. Pinho, M.F. Proença, Edge effects on the flow characteristics in a 90º tee junction. Trans. ASME, J. of Fluid Engineering 128 6 (2006) 1204-1217.

[19] A. de Tilly, J.M.M. Sousa, An experimental study of heat transfer in a two-dimensional T-junction operating at a low momentum flux ratio. International Journal of Heat and Mass Transfer 51 (2008) 941-947.

[20] J.B.W. Kok, S. van der Wal, Mixing in T-junctions. Applied Mathematical Modelling 20 (1996) 232-243.

[21] M. Lakshmiraju, J. Cui, Numerical investigation o pressure loss reduction in a power plant stack. Applied Mathematical Modelling 31 (2007) 1915-1933.

[22] W. Vicente, M. Salinas-Vazquez, C. Chavez, E. Carrizosa, Different numerical methods in the study of passive scalar transport in a pipeline X-junction. Applied Mathematical Modelling 33 (2009) 1248-1258.

[23] M.A. Leschziner, K.P. Dimitriadis, Computation of three-dimensional turbulent flow in non-orthogonal junctions by a branch-coupling method, Computer & Fluids 17 (1989) 371-396.

[24] Y. Zhao, D.E. Winterbone, A study of multi-dimensional gas flow in engine manifolds, Proc. Inst. Mech. Eng. 218 Part C D04892 (1994).

[25] C.T Shaw, D.J. Lee, S.H. Richardson, S. Pierson, Modelling the effect of plenum-runner interface geometry on the flow through an inlet system, SAE Technical paper series 2000-01-0569 (2000).

[26] G. Gan, S.B. Riffat, Numerical determination of energy losses at duct junctions, Applied energy 67 (2000) 331-340.

[27] W.H. Hager, An approximate treatment of flow in branches and bends, Procc. Inst. Mech. Eng. 198C 4 (1984) 63-69.

[28] N.I Abou-Haidar, S.L. Dixon, Pressure losses in combining subsonic flows through branched ducts. Trans. ASME, J. of Turbomachinery 114 1 (1992) 264-270.

[29] M.D. Basset, R.J. Pearson, D.E. Winterbone, R. Sierens, Steady-flow loss-coefficient estimation for exhaust manifold pulse-converter type junctions, SAE Technical paper series 1999-01-0213 (1999).

[30] D.E. Winterbone, R.J. Pearson, Theory of engine manifold design. Wave action methods for IC engines. Professional Engineering Publishing. London, 2000.

[31] T. Morimune, N. Hirayama, T. Maeda, Study of compressible high speed gas flow in piping system, Bulletin of the JSME 124 198 (1981) 2082-2089.

[32] N.I. Abou-Haidar, S.L. Dixon, Pressure losses in combining subsonic flows through branched ducts. Trans. ASME, J. of Turbomachinery 144 1 (1992) 264-270.

[33] N.I Abou-Haidar, Computational modelling of combining compressible flow through 30-150º tee junction 9 IGTI ASME COGEN-TURBO (1994) 141-150

[34] J. Pérez-García, E. Sanmiguel-Rojas, J. Hernández-Grau, A.Viedma, Numerical and experimental investigations on internal compressible flow at T-type junctions. Experimental Thermal and Fluid Science 31 (2006) 61-74.

[35] Fluent 6.0 User's guide, vol 5, Fluent Inc., Lebanon, NH 2001.

[36] D.S. Miller, Compressible Internal Flow, Fluid Eng. Series BHRA 10 (1984).

[37] J. Pérez-García, Numerical and experimental investigations on steady compressible flow at junctions. Ph D Thesis. Technical University of Cartagena, Cartagena (2006). (in Spanish) http://hdl.handle.net/10317/978

[38] Sanmiguel-Rojas E, Ortega-Casanova J, Del-Pino-Peñas C, Fernandez-Feria R. A cartesian grid finite-difference method for 2D incompressible viscous flows in irregular geometries. Journal of Computational Physics, 2005, vol 204, pp. 302-318

[39] ISO/IEC Guide 98:1995, "Guide to the Expression of Uncertainty in Measurement (GUM)", International Organization for Stand. (ISO), Geneva, Switzerland, pp. 9-78.

[40] H.W. Coleman, W. Steele, Experimentation and Uncertainty Analysis for Engineers, John Wiley & Sons., 2nd Ed., New York. ISBN 0-471-12146-0 (1999).

[41] R.E. Walpole, R.H. Myers, S.L. Myers, Probability and statistics for Engineers, Prentice Hall Hisp., 6th Ed., México. ISBN 970-17-0264-6 (1999).

[42] Freitas C.J, Ghia U., Celik,I., Roache,P., and Raad P. ASME's quest to quantify numerical uncertainty. 41st AIAA Aerospace Sciences Meeting and Exhibit, Reno, NV, 2003, January 6-9. AIAA Paper 2003-627

[43] D.A. Knoll, D.E. Keyes, Jacobian-free Newton-Krylov methods: a survey of approaches and applications. J. Computational Physics 193 (2004) 357-397.

Figure Captions

Figure 1. Evolution of the stagnation pressures in a T-junction. Extrapolated and measured quantities.

Figure 2. Notation of the *linking coefficient* for different flow configurations:
a) Combining flow b) Dividing flow

Figure 3. Comparison between experimental data, regression plane and numerical results a) for combining flow type C2 and b) for dividing flow type D2

Figure 4. Regression plane and numerical results for a) combining flow type C2 and c) for dividing flow type D2. Lateral view for C2 and D2 in b) and d), respectively.

Figure 5. Regression plane and numerical results for a) combining flow type $C1$, coefficient $\hat{K}_1$, b) combining flow type $C1$, coefficient $\hat{K}_2$, c) dividing flow type $D1$, coefficient $\hat{K}_1$ and d) dividing flow type $D1$, coefficient $\hat{K}_2$.

Table Captions

Table 1. Global correlations obtained from numerical results.

Table C.1. Geometrical characteristics of the studied meshes at 90 degree T-junction. Computational domain reduced due to double symmetry plane

in combining flow type C2 q=0.5.

Table C.2. Estimation of the numerical uncertainty. $G_3 = 0.128$ kg/s.

Table C.3. Obtained values of GCI in % to estimate the numerical uncertainty.

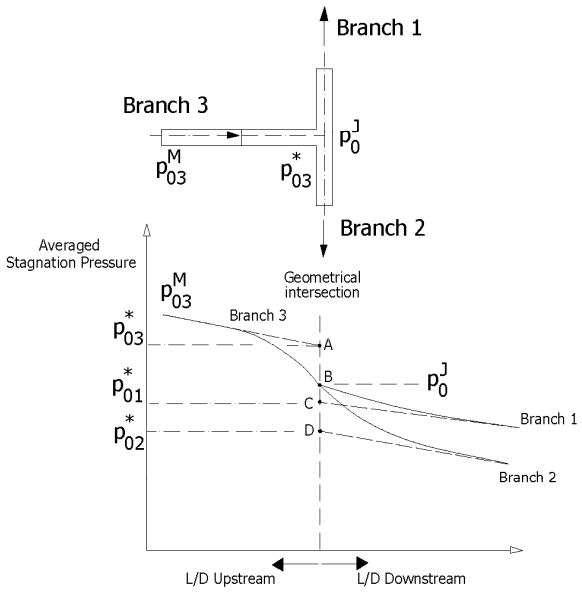

Fig.1

Fig.2

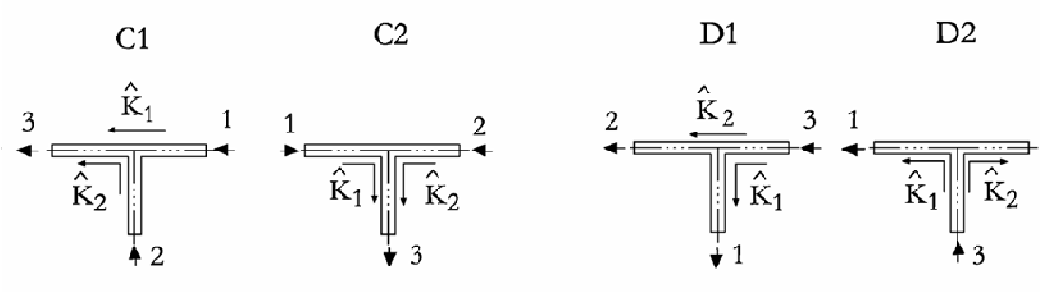

Fig.3(a)

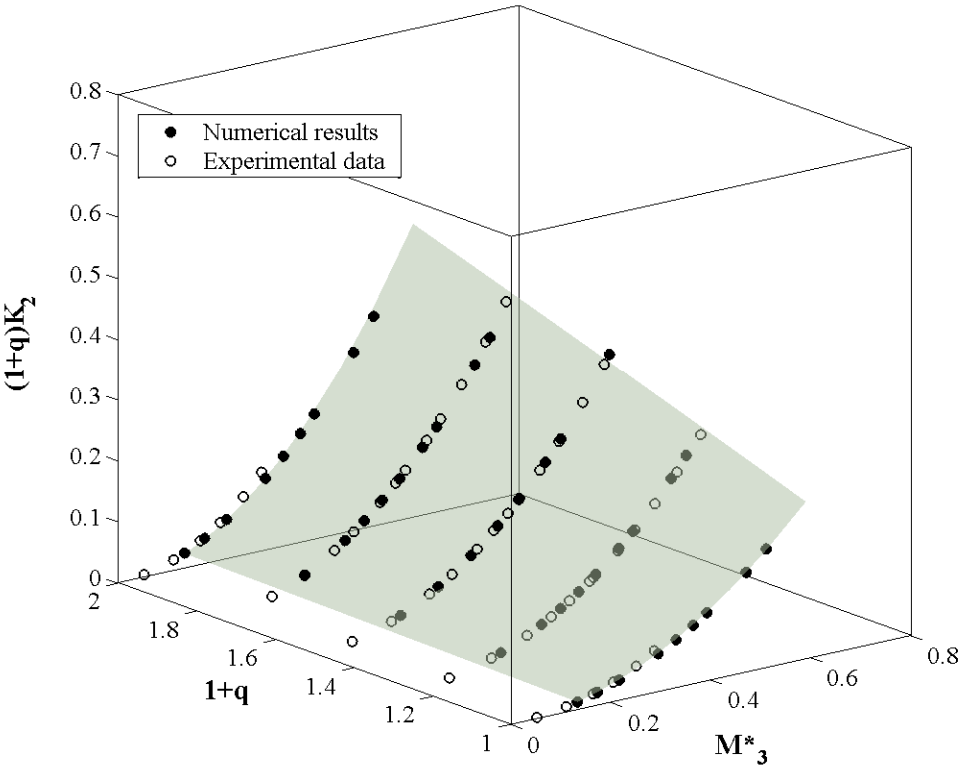

Fig.3(b)

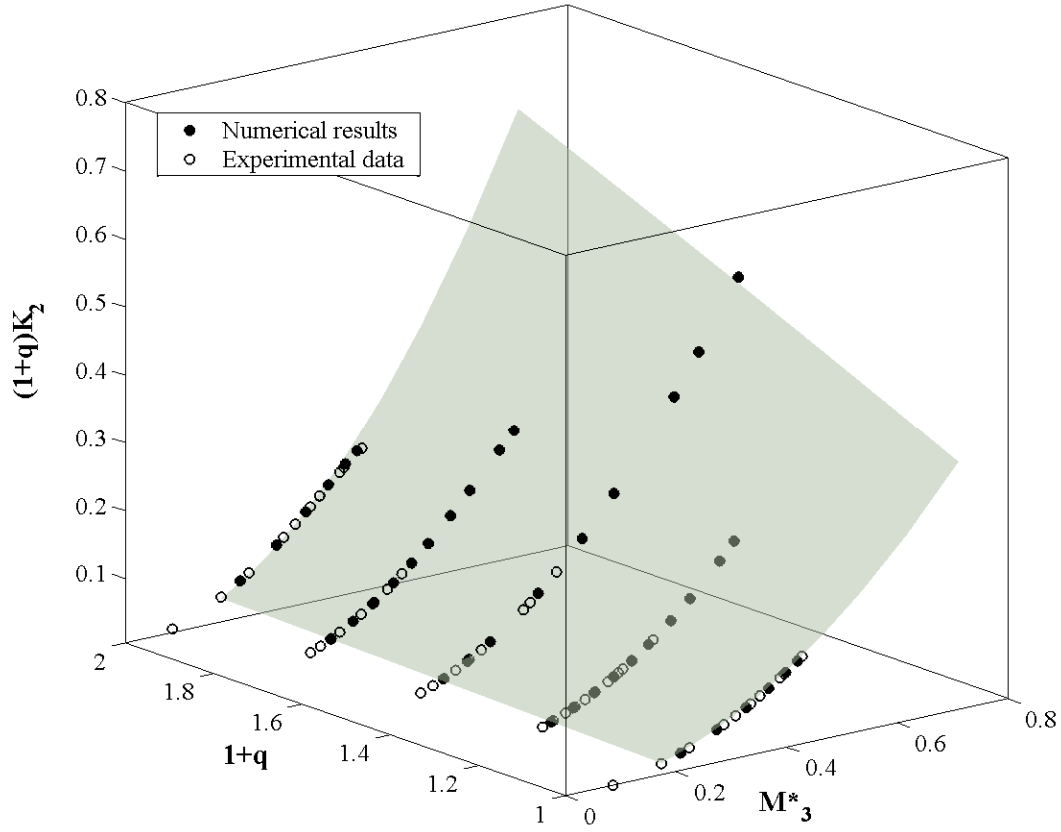

Fig.4(a)

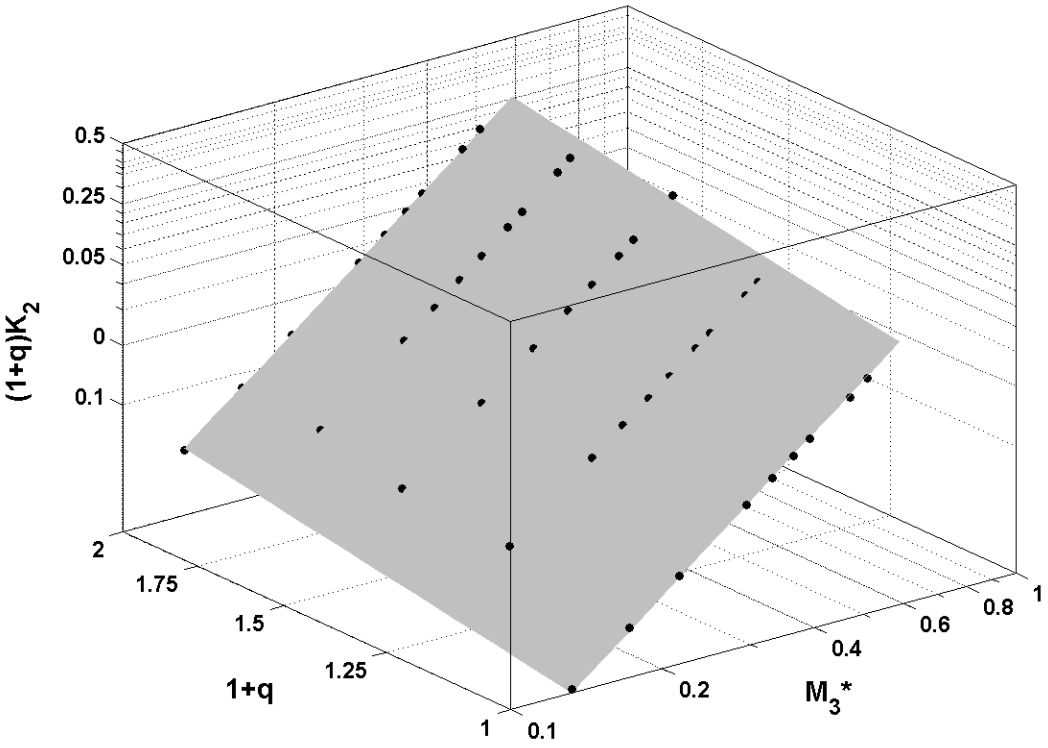

Fig.4(b)

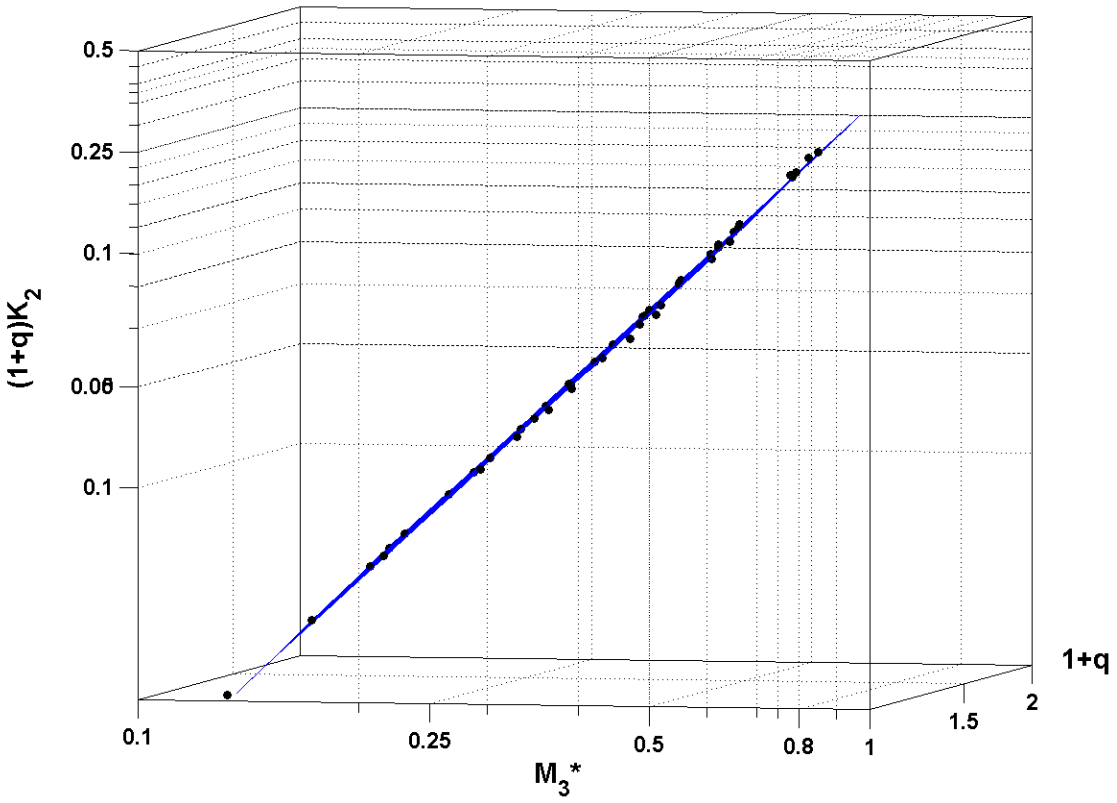

Fig.4(c)

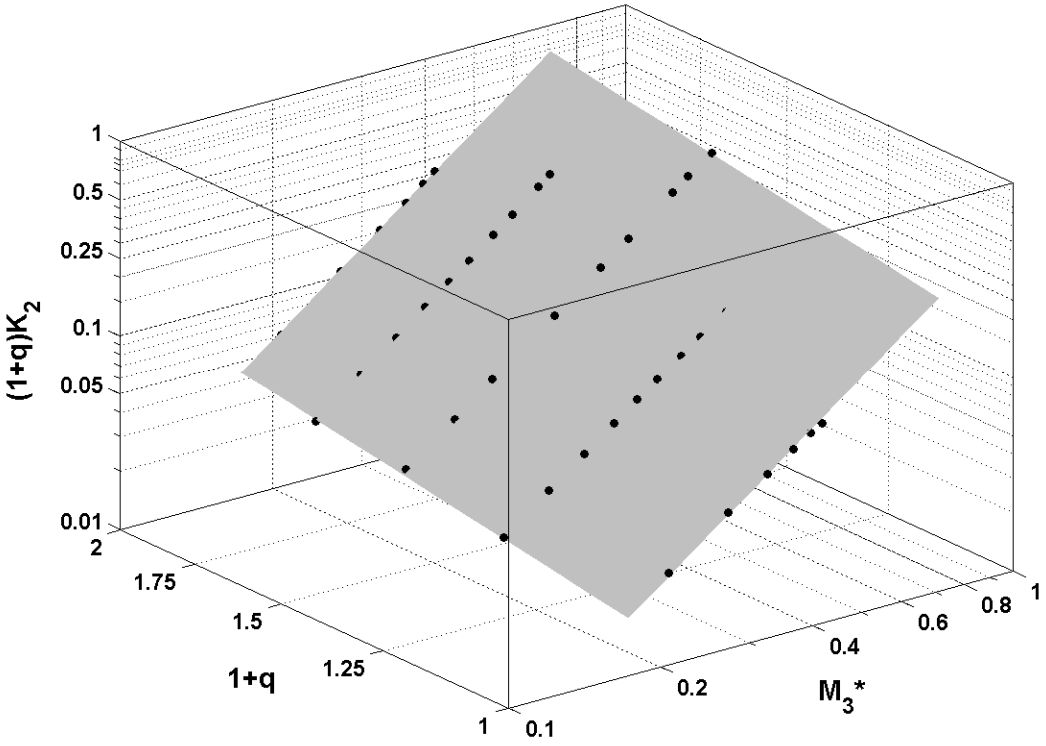

Fig.4(d)

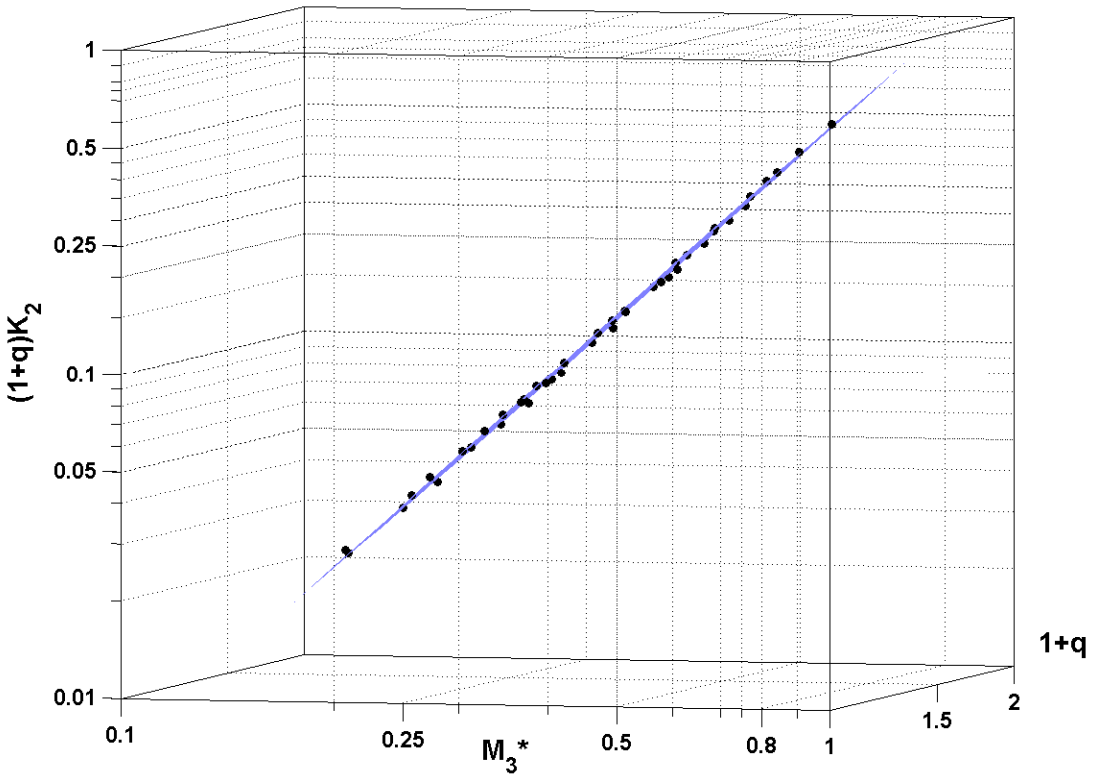

Fig.5(a)

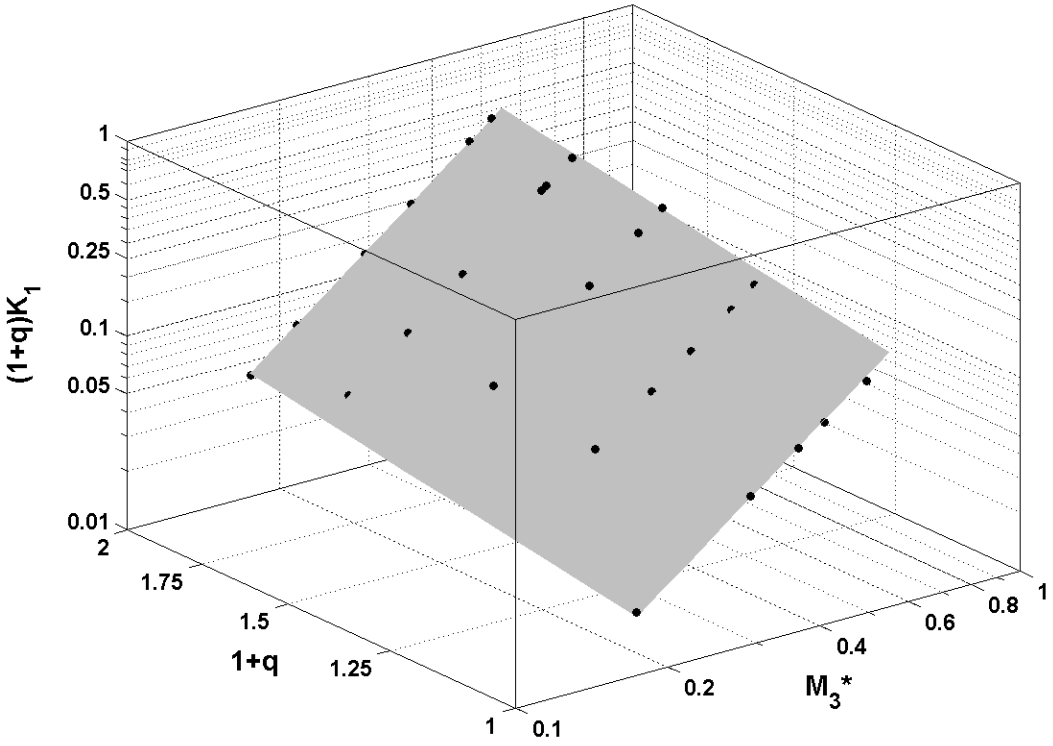

Fig.5(b)

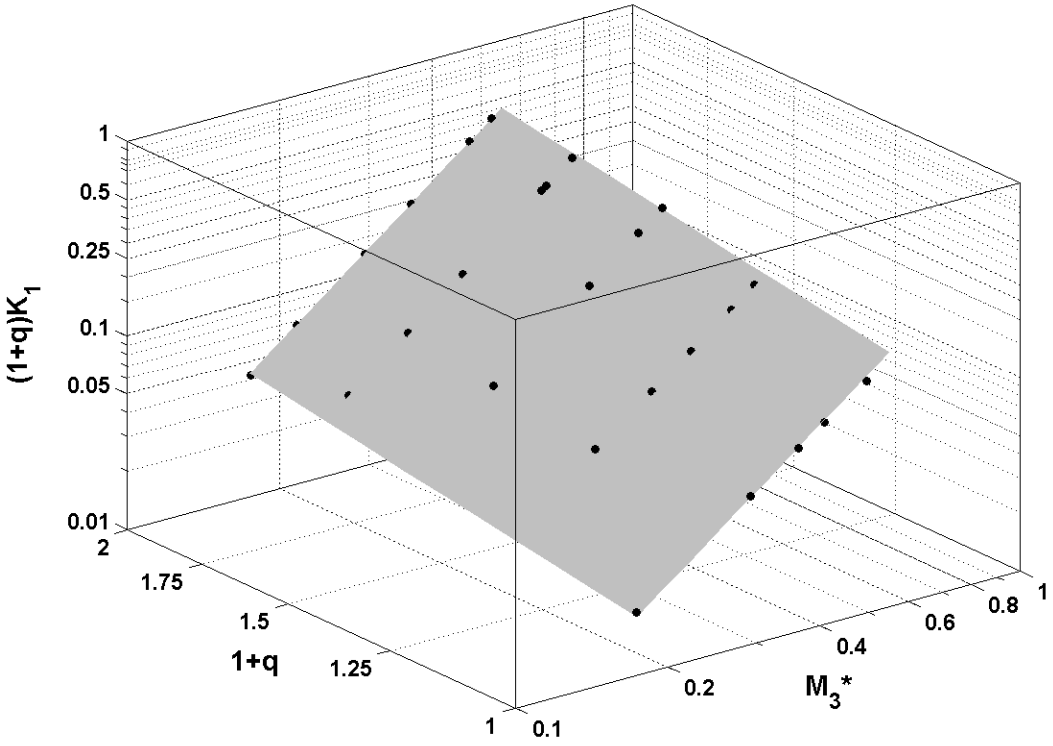

Fig.5(c)

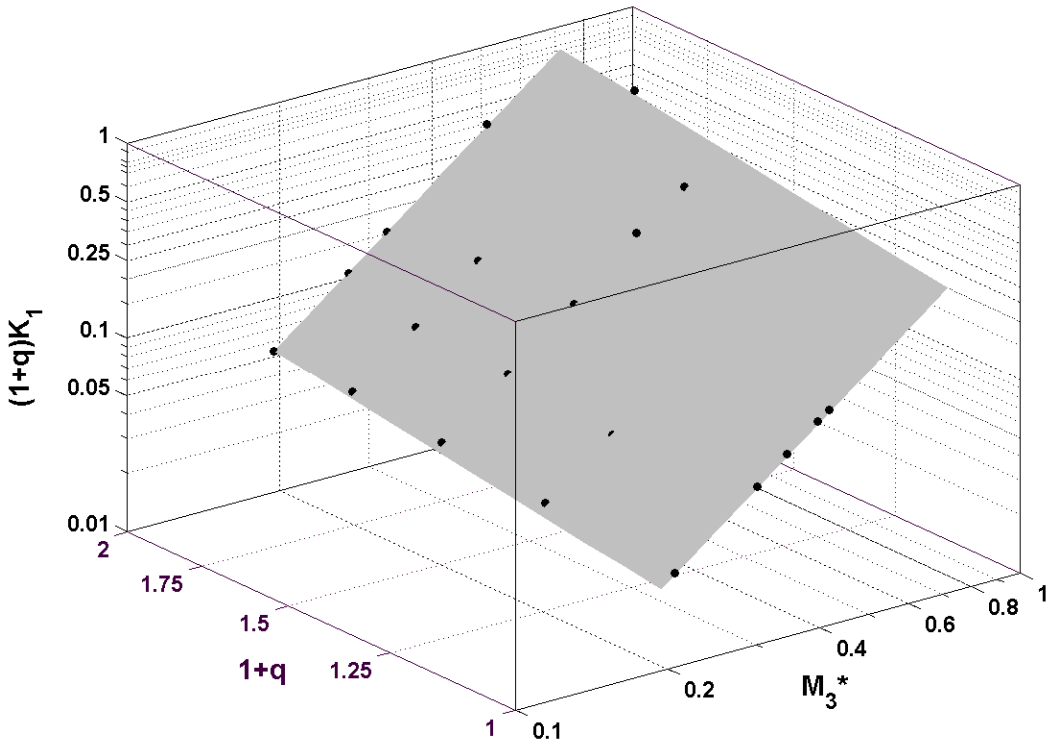

Fig.5(d)

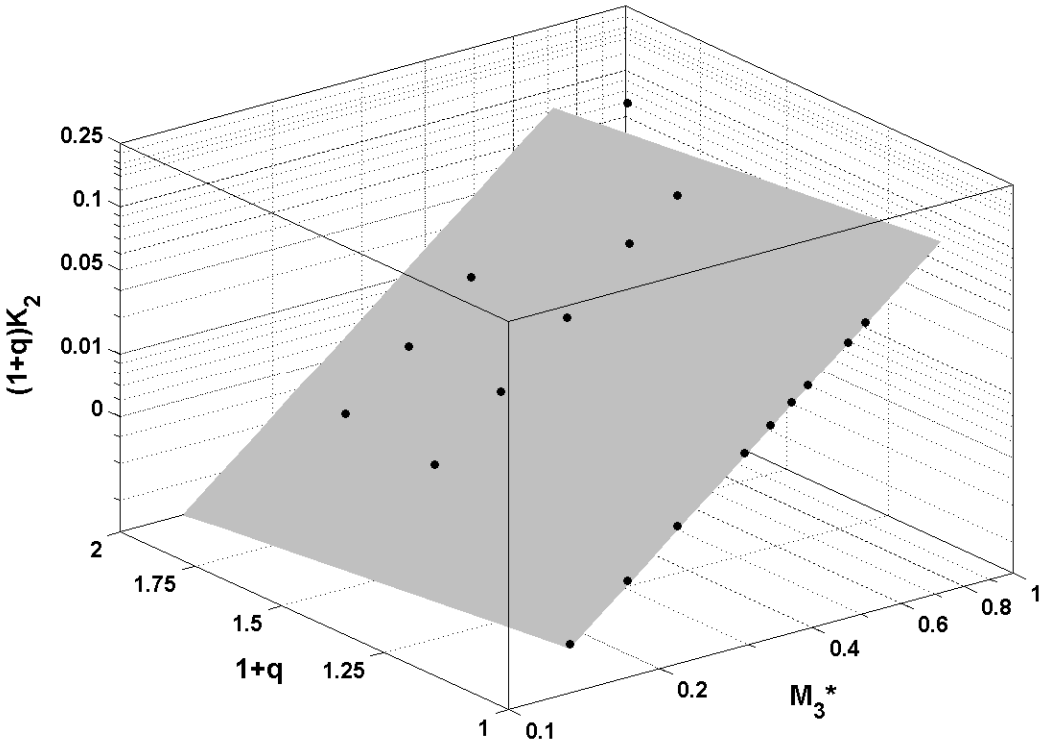

Flow type	Numerical correlation	Expanded Uncertainty (95% CI)	Correlation coefficient
C1	$\hat{K}_1 = 0.6871 M_3^{*2.0283}(1+q)^{0.1296}$	5.75 %	$R^2 = 1.0000$
	$\hat{K}_2 = 0.7559 M_3^{*2.0378}(1+q)^{-0.0392}$	4.35 %	$R^2 = 0.9996$
C2	$\hat{K}_2 = 0.7504 M_3^{*2.0223}(1+q)^{-0.0957}$	3.54 %	$R^2 = 1.0000$
D1	$\hat{K}_1 = 0.7312 M_3^{*2.0374}(1+q)^{0.0398}$	4.64 %	$R^2 = 0.9997$
	$\hat{K}_2 = 0.6718 M_3^{*1.9543}(1+q)^{0.0242}$	6.25 %	$R^2 = 0.9998$
D2	$\hat{K}_2 = 0.7307 M_3^{*1.9927}(1+q)^{-0.1538}$	3.99 %	$R^2 = 1.0000$

Number of elements	Coarse Mesh	Normal Mesh	Fine Mesh
N° of cells	36.840	88.416	294.720
N° of nodes	45.532	121.733	421.494
Δx (mm)	0.8571	0.4286	0.2143
Δy (mm)	0.8571	0.4286	0.2143
Δz (mm)	1.7143	0.8571	0.4286
h_m (Representative cell size, mm)	1.0800	0.5400	0.2700

	$M_3\ (p<1)$	$M_3\ (p=1)$
r_{21}	2	2
r_{32}	2	2
ϕ_1	0.5749	0.5749
ϕ_2	0.6290	0.6290
ϕ_3	0.6311	0.6311
p	-4.6610	1
ε_{21}	0.0859	0.0859
ε_{32}	0.0034	0.0034
ϕ_{ext}^{21}	0.6312	0.5286
ϕ_{ext}^{32}	0.6312	0.6268
e_a^{21}	0.0940	0.0940
e_a^{32}	0.0034	0.0034
e_{ext}^{21}	0.0892	0.1038
e_{ext}^{32}	0.00014	0.0068
$GCI_{coarse-normal}$	-12.24 %	11.75 %
$GCI_{normal-fine}$	-0.44 %	0.43 %

Mass Flow Rate (kg/s)	M_3 Coarse-Normal ($p < 1$)	M_3 Normal-Fine ($p < 1$)	M_3 Coarse-Normal ($p = 1$)	M_3 Normal-Fine ($p = 1$)
0.016	-15.42	0	15.42	0
0.024	-15.24	0.05	15.18	0.05
0.04	-14.38	-0.02	14.37	0.02
0.056	-13.25	-0.32	12.9	0.31
0.064	-12.24	-0.44	11.75	0.43
0.088	-6.71	-0.92	5.76	0.79
0.1	-4.11	-1.19	2.9	0.84

Flow type	Numerical correlation	Expanded Uncertainty (95% CI)	Correlation coefficient
C1	$\hat{K}_1 = 0.6871 M_3^{*2.0283}(1+q)^{0.1296}$	5.75 %	$R^2 = 1.0000$
	$\hat{K}_2 = 0.7559 M_3^{*2.0378}(1+q)^{-0.0392}$	4.35 %	$R^2 = 0.9996$
C2	$\hat{K}_2 = 0.7504 M_3^{*2.0223}(1+q)^{-0.0957}$	3.54 %	$R^2 = 1.0000$
D1	$\hat{K}_1 = 0.7312 M_3^{*2.0374}(1+q)^{0.0398}$	4.64 %	$R^2 = 0.9997$
	$\hat{K}_2 = 0.6718 M_3^{*1.9543}(1+q)^{0.0242}$	6.25 %	$R^2 = 0.9998$
D2	$\hat{K}_2 = 0.7307 M_3^{*1.9927}(1+q)^{-0.1538}$	3.99 %	$R^2 = 1.0000$